Regularized anisotropic motion-by-curvature in phase-field theory: Interface phase separation of crystal surfaces

Thomas Philippe, Hervé Henry, and Mathis Plapp
Laboratoire de Physique de la Matière Condensée, CNRS, Ecole polytechnique, Institut Polytechnique de Paris, 91120 Palaiseau, France

(Received 22 April 2022; accepted 26 August 2022; published 12 September 2022)

The kinetic equation for anisotropic motion-by-curvature is ill posed when the surface energy is strongly anisotropic. In this case, corners or edges are present on the Wulff shape, which span a range of missing orientations. In the sharp-interface problem the surface energy is augmented with a curvature-dependent term that rounds the corners and regularizes the dynamic equations. This introduces a new length scale in the problem, the corner size. In phase-field theory, a diffuse description of the interface is adopted. In this context, an approximation of the Willmore energy can be added to the phase-field energy so as to regularize the model. In this paper, we discuss the convergence of the Allen-Cahn version of the regularized phase-field model toward the sharp-interface theory for strongly anisotropic motion-by-curvature in three dimensions. Corners at equilibrium are also compared to theory for different corner sizes. Then we investigate the dynamics of the faceting instability, when initially unstable surfaces decompose into stable facets. For crystal surfaces with trigonal symmetry, we find the following scaling law $L \sim t^{1/3}$, for the growth in time t of a characteristic morphological length scale L, and coarsening is found to proceed by either edge contraction or cube removal, as in the sharp-interface problem. Finally, we study nucleation of crystal surfaces in a two-phase system, as for a terrace-and-step surface. We find that, as compared with saddle-point nucleation, ridge crossing is dynamically favored. However, the induced nucleation mechanism, when a facet induces at its wake formation of additional facets, is not evidenced with a type-A dynamics.

DOI: 10.1103/PhysRevE.106.034119

I. INTRODUCTION

In material science, motion-by-curvature was introduced by Mullins [1] in the framework of grain boundary motion. Following this theory, in the absence of any other driving force, the normal velocity of isotropic interfaces v_n is given by

$$v_n = M\gamma(k_1 + k_2), \tag{1}$$

where γ is the surface energy, k_1 and k_2 are the principal curvatures of the surface, M is the interfacial mobility, and $\gamma(k_1 + k_2)$ corresponds to the free-energy difference (or chemical potential in single component systems) between the energy of the flat surface and that of the curved one. The formula of the chemical potentials was then extended by Herring for anisotropic surface energy [2,3], which leads to the following expression for the velocity:

$$v_n/M = \gamma(k_1 + k_2) + \frac{\partial^2\gamma}{\partial {n_1}^2}k_1 + \frac{\partial^2\gamma}{\partial {n_2}^2}k_2, \tag{2}$$

where γ is now a function of the outwards unit normal to the interface $\vec{n}$; n_1 and n_2 denote the orthogonal components of $\vec{n}$ along the tangent vectors $\vec{t}_1$ and $\vec{t}_2$, taken here in the principal directions of the surface. One may also express motion-by-curvature from the interface stiffness tensor [4,5]:

$$v_n/M = \left(\gamma\mathbf{P} + \frac{\partial^2\gamma}{\partial\vec{n}^2}\right)\cdot\mathbf{L}, \tag{3}$$

where $\mathbf{P} = \mathbf{I} - \overrightarrow{n} \otimes \overrightarrow{n}$ is the projection onto the surface and $\mathbf{I}$ the identity matrix. $\mathbf{L} = -\vec{\nabla}_S\vec{n}$ is the curvature tensor, from which the total curvature K (twice the mean curvature) at a point of the surface can be evaluated, $K = \mathrm{tr}(\mathbf{L}) = k_1 + k_2$. $\vec{\nabla}_S$ is the surface gradient.

There are situations of interest in which the motion of an interface is independent of the bulk phases and is only due to motion-by-curvature. Models to describe such cases are based on Eq. (2) or equivalently on Eq. (3). However, the later are ill posed for realistic interfacial energies [6–9]. Indeed, for a crystal, anisotropy of surface energy reflects the dependence of the surface orientation with respect to the crystallographic axes. This dependence is visible on equilibrium shapes, for instance. Emergence of facets on the equilibrium shape of a crystal is due to cusps in the surface energy. In presence of cusps, Eq. (2) is not defined since the surface energy is nondifferentiable [10]. Issues may also arise when the surface energy is differentiable. For moderate anisotropy strength, the equilibrium shape is smooth, with high-energy directions occupying a smaller fraction of the surface area than low-energy directions. However, when the surface energy is strongly anisotropic, and nonconvex [7], some orientations are missing on the equilibrium shape, which now contains sharp corners and edges. At the corner, a phase transition operates, known as the interfacial phase transition. A surface initially oriented along missing orientations will decompose into the stable orientations that are determined by the equilibrium condition for a corner [7]. This is perfectly analogous to the phase separation of a homogeneous binary or ternary

mixture. The corresponding missing orientations may be either metastable or unstable by opposition to the orientations on the equilibrium shape that are stable. In the metastable case, formation of stable surfaces occurs by nucleation and growth, whereas unstable surfaces decompose into stable ones by spinodal decomposition. The later phenomenon is known as the faceting instability or spinodal of facets. In both cases, the kinetic equation becomes ill posed (backward parabolic) in the corner region and needs to be regularized. In this article we will limit ourselves to this issue: a differentiable surface energy with nonconvex parts.

In the sharp interface theory, regularization is done by introducing a new length scale in the problem, the corner size [5,11,12]. This can be achieved by making the surface energy dependent on the interface curvature in two or three dimensions [3–5,11–14]. This curvature dependence also gives an energy to corners (and edges). In three dimensions, the regularized version of the kinetic equation is given by [14]:

$$v_n/M = -\vec{\nabla}_S \cdot \vec{\xi} - \beta\left(\Delta_S K - 2KG + \frac{K^3}{2}\right), \qquad (4)$$

where β is a parameter that is introduced in the regularized form of the surface energy: $\gamma(\vec{n}) + \beta K^2/2$, with as before $K = k_1 + k_2$, k_1 and k_2 being again the principal curvatures of the surface. $G = k_1 k_2$ is the Gaussian curvature and Δ_S denotes the surface Laplacian. In the above equation, Herring's result [Eq. (2)] was reformulated using the well-known Cahn-Hoffman $\vec{\xi}$ vector [15,16], defined as $\vec{\nabla}[r\gamma(\vec{n})]$ with a position vector $\vec{r} = r\vec{n}$ [15]. $\vec{\nabla}_S \cdot \vec{\xi}$ is the surface divergence of the $\vec{\xi}$ vector. We will use Cahn-Hoffman's formalism in this article, as we will derive a diffuse-interface version of the $\vec{\xi}$ vector in our phase-field model. At equilibrium, the interface must therefore satisfy the following condition:

$$-\vec{\nabla}_S \cdot \vec{\xi} - \beta\left(\Delta_S K - 2KG + \frac{K^3}{2}\right) = 0. \qquad (5)$$

Regularization of models for strongly anisotropic surface energy has been the subject of intense research in both the sharp-interface theory [4,5,11–13,17–26] and the diffuse interface description [10,27–38]. For a complete picture, the reader is invited to read Ref. [13] for more details on regularization in sharp interface theories and Ref. [30] for the description of the methods that have been proposed in the phase-field framework. We also need to mention that another possibility of regularization is to convexify the surface energy [39,40]: The energy is modified so that the region that contains the missing orientations becomes convex, while the construction preserves the orientations on both sides of the corners. This method is computationally attractive but cannot reproduce the decomposition of an unstable surface into facets since the nonconvex part of the energy is missing. Therefore, the method that is investigated in the following regularizes the free energy and preserves the phase transition at the interface [41]. To our knowledge, no demonstration of the equivalence between the regularized phase-field model and sharp-interface theory [Eq. (5)] is currently available in three dimensions. We establish such an equivalence in the following work.

In this paper, the energy of the phase-field model relies on the formulation proposed by Torabi *et al.* [30] that is regularized using an approximation of the Willmore energy [42–47] with an additional term in the free energy that approximates the square of the mean curvature. In the original model [30] the Cahn-Hilliard equation is employed to mimic the surface diffusion equation. In our model, the dynamics is given by the Allen-Cahn equation and there is no other driving force added to the interface motion. Therefore, the motion is purely driven by capillarity. Furthermore, contrary to our previous study on crystal growth [48], the present study is made in three dimensions. Extending the regularized problem to three dimensions is known to be nontrivial [4,13], and, therefore, we choose to present this work in a separate paper. Moreover, the method that is employed to show the convergence of the phase-field model toward the sharp-interface theory is also different from that we employed in the two-dimensional version of the model [48] where we used the classical method of matched asymptotic expansions in the Allen-Cahn equation. In the present analysis, we start from the stress tensor [49], use one of its known properties, the stress tensor being divergence-free at equilibrium, and then perform the asymptotics to demonstrate the convergence toward Eq. (5). It avoids extensive calculations with curvilinear coordinates [50,51] by using some known properties of differential geometry [4].

Finally, we note that our main goal is to build a phase-field model that reproduces regularized anisotropic motion-by-curvature [Eq. (4)] in the limit of small interface thickness. Indeed, we are interested in a generic model that mimics pure motion-by-curvature [Eq. (4)], which then can be applied and extended to many different interfaces and problems. As an illustration, we investigate the faceting instability [41], whose sharp-interface properties are well known for the evaporation-condensation mechanism [17,25]. We also study nucleation from metastable surfaces, for which little is known, even in the simplest dynamics settings [21]. In Sec. II we present the regularized phase-field model and show its convergence toward Eq. (5) from the stress tensor [29,49,52,53]. We then investigate, in Sec. III, the effect of the regularization parameter on the corner morphology, at equilibrium, and compare the phase-field results to theory [14,17] for a given anisotropy function. The dynamics of the faceting instability is investigated in Section IV, as well as nucleation of crystal surfaces. In Sec. V, we summarize the main results.

II. PHASE-FIELD MODEL

We present here the main equations of the regularized phase-field model and show its asymptotic convergence, in three dimensions, toward the sharp-interface theory [Eq. (5)]. For this purpose, we use the stress tensor, which provides a mechanical interpretation of the phase-field model being, by definition, divergence-free at equilibrium. Before deriving the expression for the diffuse stress tensor in the regularized theory, let us first describe the governing equations of the phase-field model.

A. Governing equations

The free energy, for the phase-field u, is given by [30]:

$$F = \int f dV, \tag{6}$$

where f is the the classical phase-field energy to which a regularization term is added:

$$f = \frac{\Gamma(\vec{n})}{\varepsilon}\left[\Psi(u) + \frac{\varepsilon^2}{2}|\vec{\nabla}u|^2\right] + \frac{\alpha^2}{2\varepsilon}\left[\frac{\Psi_u(u)}{\varepsilon} - \varepsilon\Delta u\right]^2, \tag{7}$$

where ε is the interface width. In this study, $u = -1$ and $u = +1$ in the bulk phases. $H\Psi(u)$ is a double-well energy density, with H the height of the barrier, here $\Psi(u) = \frac{1}{2}(1-u^2)^2$. The dimensionless function $\Gamma(\vec{n})$ encodes anisotropy, with the normal vector defined as $\vec{n} = \vec{\nabla}u/|\vec{\nabla}u|$, and sets the magnitude of the surface energy $\gamma_0\Gamma(\vec{n}) = \widetilde{a}\varepsilon H\Gamma(\vec{n})$ with $\widetilde{a} = \frac{4}{3}$ for our choice of $\Psi(u)$ [48]. γ_0 is a constant. The last term in Eq. (7) regularizes the free energy and introduces a new length scale, the bending length $\alpha = \sqrt{\beta/\gamma_0}$. This term is an approximation of the Willmore energy and is due to De Giorgi [42–47]. The Allen-Cahn equation sets the dynamics:

$$\partial_t u = -\frac{1}{\tau'}\varepsilon\frac{\delta F}{\delta u}, \tag{8}$$

where

$$\frac{\delta F}{\delta u} = \frac{1}{\varepsilon}[\Gamma(\vec{n})\Psi_u(u) - \varepsilon^2\vec{\nabla}\cdot\vec{m}] + \frac{\alpha^2}{\varepsilon^3}[\Psi_{uu}(u)w(u) - \varepsilon^2\Delta w(u)], \tag{9}$$

with $w(u) = \Psi_u(u) - \varepsilon^2\Delta u$ and

$$\vec{m} = \Gamma(\vec{n})\vec{\nabla}u + \mathbf{P}\cdot\vec{\nabla}_n\Gamma(\vec{n})\left[\frac{\Psi(u)}{\varepsilon^2|\vec{\nabla}|} + \frac{1}{2}|\vec{\nabla}u|\right]. \tag{10}$$

$\mathbf{P}$ is the projection matrix: $\mathbf{P} = \mathbf{I} - \overrightarrow{n}\otimes\overrightarrow{n}$; $\mathbf{I}$ is the identity matrix and $\overrightarrow{\nabla}_n = \frac{d}{d\overrightarrow{n}}$.

Lengths are then rescaled by a macroscopic distance D such as $\widetilde{\varepsilon} = \varepsilon/D \ll 1$ and $\widetilde{\alpha} = \alpha/D \ll 1$. Time is rescaled by $\tau = \tau'/\varepsilon^2$. τ' is related to the sharp-interface mobility M by $\tau' = \varepsilon/(\widetilde{a}HM)$, such that $\tau = D^2/(M\gamma_0)$. In the following, tildes are omitted for sake of clarity. The dimensionless evolution equation reads:

$$\varepsilon^4\partial_t u = -\varepsilon^2[\Gamma(\vec{n})\Psi_u(u) - \varepsilon^2\vec{\nabla}\cdot(-|\vec{\nabla}u|\vec{\Xi})] + \alpha^2[\varepsilon^2\Delta w(u) - \Psi_{uu}(u)w(u)]. \tag{11}$$

In Eq. (11), the asymptotic result near the interface at equilibrium has been used, $\Psi(u) = \varepsilon^2|\vec{\nabla}u|^2/2$, to evaluate $\vec{m}$. Introducing this result makes the model nonvariational. However, up to third order [48], the asymptotics of the variational model is identical. Therefore, the following analysis remains valid for the variational model also. In this approximation, $\vec{m}$ also reads $\vec{m} = -|\vec{\nabla}u|\vec{\Xi}$ with $\vec{\Xi} = -\Gamma(\vec{n})\vec{n} - \mathbf{P}\cdot\vec{\nabla}_n\Gamma(\vec{n})$, which can be identified to the dimensionless vector $\vec{\Xi}$ introduced by Cahn and Hoffman [16].

B. Stress tensor

Now, inspired by Wheeler and McFadden [29,49], we compute a stress tensor; that is by definition divergence free at equilibrium, since forces acting on the interface must balance each other. The stress tensor is of special interest as it provides a mechanical interpretation of the phase-field model. In this context it has been shown that the stress tensor is in general not symmetric. The presence of surface energy anisotropy induces a body couple throughout the diffuse interface as the system can reduce its surface energy by curve shortening (as in the isotropic case) but also by local rotation. Consider the energy density $\Lambda(\vec{x}, u, \vec{\nabla}u, \Delta u)$, which has explicit dependence on the scalar u, its gradient $\vec{\nabla}u$, its Laplacian Δu, and the position vector $\vec{x}$. The Euler-Lagrange equation can be written as the divergence of a tensor:

$$0 = \vec{\nabla}\cdot\mathbf{S}, \tag{12}$$

with

$$\mathbf{S} = \vec{\nabla}u\otimes\frac{\partial\Lambda}{\partial\vec{\nabla}u} - \Lambda\mathbf{I} + \frac{\partial\Lambda}{\partial\Delta u}\vec{\nabla}\vec{\nabla}u - \vec{\nabla}u\otimes\vec{\nabla}\frac{\partial\Lambda}{\partial\Delta u}, \tag{13}$$

where $\mathbf{I}$ is the unit tensor. The calculation, originally made by Wheeler [29], is given in the Appendix for sake of completeness. Applied to the present formulation of the energy density, Eq. (7), we obtain for the stress tensor:

$$\mathbf{S} = -\varepsilon|\vec{\nabla}u|\vec{\nabla}u\otimes\vec{\Xi} - \Lambda\mathbf{I} + \frac{\alpha^2}{\varepsilon}(\vec{\nabla}u\otimes\vec{\nabla}w - w\vec{\nabla}\vec{\nabla}u), \tag{14}$$

and its dimensionless form ($\mathbf{S}\to\varepsilon\mathbf{S}$) is given by

$$\mathbf{S} = -\varepsilon^2|\vec{\nabla}u|\vec{\nabla}u\otimes\vec{\Xi} - \Gamma(\vec{n})\left[\Psi(u) + \frac{\varepsilon^2}{2}|\vec{\nabla}u|^2\right]\mathbf{I} - \frac{\alpha^2}{2\varepsilon^2}w^2\mathbf{I} + \alpha^2(\vec{\nabla}u\otimes\vec{\nabla}w - w\vec{\nabla}\vec{\nabla}u), \tag{15}$$

where lengths have been scaled by D, and again tildes are omitted for sake of clarity. Then, we introduce a distance d to perform the asymptotics, d being the signed distance from point x of region Ω to the front ζ, defined as the zero-level set of the phase-field u. In the region denoted Ω_+, $d > 0$ and $d < 0$ in Ω_-. Using the asymptotic result near the interface $\Psi(u) \sim \varepsilon^2|\vec{\nabla}u|^2/2$, we get for the dimensionless stress tensor:

$$\mathbf{S} = \varepsilon^2 u_d{}^2[-\vec{n}\otimes\vec{\Xi} - \Gamma(\vec{n})\mathbf{I}] - \frac{\alpha^2}{2\varepsilon^2}w^2\mathbf{I} + \alpha^2(\vec{\nabla}u\otimes\vec{\nabla}w - w\vec{\nabla}\vec{\nabla}u), \tag{16}$$

with u_d the first derivative of u with respect to the signed distance d. We see that the presence of surface energy anisotropy leads to a body couple distribution given by $\vec{\Xi}\times\vec{n}$. The latter vanishes in the isotropic case, as $\vec{\Xi}$ is parallel to $\vec{n}$. Therefore, anisotropy induces a body couple throughout the interface indicating that the interface can reduce its surface energy by local rotation and curve shortening [49]. Then, we expand the functions u and w far from the front ζ:

$$u(x) \sim u_0 + \varepsilon u_1 + \varepsilon^2 u_2 + ..., \tag{17}$$

$$w(x) \sim w_0 + \varepsilon w_1 + \varepsilon^2 w_2 + ... \tag{18}$$

In a small neighborhood of ζ, we define the stretched normal distance to the front $z = d/\varepsilon$, and look for inner expansions valid for a point near the front:

$$u(x) = U(z,x) \sim U_0 + \varepsilon U_1 + \varepsilon^2 U_2 + ..., \tag{19}$$

$$w(x) = W(z,x) \sim W_0 + \varepsilon W_1 + \varepsilon^2 W_2 + ... \tag{20}$$

Classically, the quantities depending on (z, x) are assumed to not change when x varies normal to the front ζ with z held fixed [54]. Then, the inner and outer expansions are related by matching conditions such that [42]:

$$(u_0 + \varepsilon u_1 + ...)(x + \varepsilon z\vec{n}) = (U_0 + \varepsilon U_1 + ...)(z,x). \tag{21}$$

The left-hand side is expanded in powers of ε as $\varepsilon z \to 0$ and $z \to \pm\infty$, the following conditions are obtained for the function u and U, and analogous conditions are obtained for w and W [42]:

$$u_0^{\pm} = \lim_{z\to\pm\infty} U_0, \tag{22}$$

$$\lim_{z\to\pm\infty} \left(u_1^{\pm} + z\vec{n}\cdot\vec{\nabla}u_0^{\pm}\right) = \lim_{z\to\pm\infty} U_1, \tag{23}$$

$$\lim_{z\to\pm\infty} \left(u_2^{\pm} + z\vec{n}\cdot\vec{\nabla}u_1^{\pm} + \frac{z^2}{2}D_{\vec{n}}^2 u_0^{\pm}\right) = \lim_{z\to\pm\infty} U_2, \tag{24}$$

where $u_k^{\pm}$ denotes $\lim_{\varepsilon z\to 0^{\pm}} u_k$ and $D_{\vec{n}}$ is the directional derivative along the normal to the interface $\vec{n}$. Moreover, in this coordinate system, we have:

$$\vec{\nabla}u = \vec{\nabla}_x U + \frac{1}{\varepsilon}U_z\vec{n}. \tag{25}$$

Using the classical method of matched asymptotic expansions [55], and substituting the expansions for U and W in Eq. (11), it can be shown from the matching conditions that, up to second order in ε, the functions U and W can be written as:

$$U = U_0 = \tanh z, \tag{26}$$

$$W = \varepsilon W_1 = -K\varepsilon U_{0,z}, \tag{27}$$

as $U_1 = 0$ and $W_0 = 0$ [42,48]. K is the total curvature of the front at the projection of x on ζ. The calculation has been made by Loreti and March in the isotropic case for the Willmore energy [42], and we performed a similar analysis in two dimensions for the anisotropic case [48]. When the surface presents a corner, the derivation requires $\varepsilon \ll \alpha$ [48,56]. As in the two-dimensional case, we find that anisotropy does not intervene in the calculation of the functions U_0, U_1, W_0, and W_1 in three dimensions. The functions U_2 and W_2 have also been calculated in Ref. [48] but are not needed in the calculation that follows. As we have derived the expression for the stress tensor and since the functions U and W are known, we can use a pillbox argument and the property $\vec{\nabla}\cdot\mathbf{S} = 0$ to establish the equilibrium condition, at leading order in ε.

Consider a pillbox enclosing a portion of the surface such as the top and bottom parts of the pillbox are above the surface at height $-h$ and below it at height $+h$ (Fig. 1). The pillbox intersects perpendicularly the contours of u. Its volume is negligible on the outer scales but the variations of the phase field u are fully contained within the pillbox, i.e., $\varepsilon \ll h$. The results of the asymptotic analysis [Eq. (26) and Eq. (27)], used in the following calculation, also need $\varepsilon \ll \alpha$ [48,56]. Thus, we require $\varepsilon \ll h \ll \alpha$. We first apply the divergence theorem:

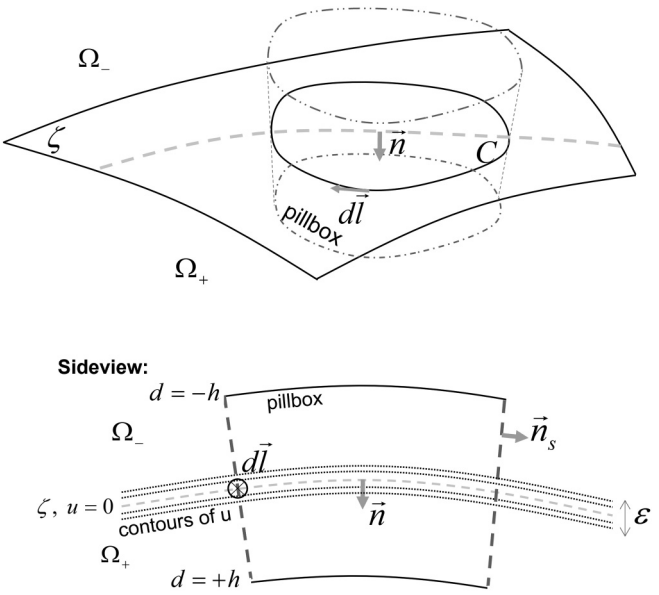

FIG. 1. Schematic of the surface, with the pillbox enclosing a portion of it, the top and bottom parts of the pillbox are above the surface at height $-h$ and below it at height $+h$. The pillbox intersects perpendicularly the contours of u. Its volume is negligible on the outer scales but the variations of the phase field u are fully contained within the pillbox, i.e., $\varepsilon \ll h$.

$$\int_{S_p} \mathbf{S}\cdot\vec{n}_p dA = 0, \tag{28}$$

where S_p is the surface of the pillbox and $\vec{n}_p$ the normal to the surface of the pillbox. The contributions from the top and bottom surfaces vanish as the phase field u is constant far from the interfacial region. Only remain the contributions from the side surface. We denote $\vec{n}_s$ the normal on the side surface of the pillbox, S_s. Thus,

$$\int_{S_p} \mathbf{S}\cdot\vec{n}_p dA = \int_{S_s} \mathbf{S}\cdot\vec{n}_s dA. \tag{29}$$

The surface integral over the side of the pillbox is written as a double integral in terms of a line integral on the physical surface and an integral in the normal direction [52,57]:

$$\int_{S_s} \mathbf{S}\cdot\vec{n}_s dA = \oint_C \int_{-h}^{h} \mathbf{S}\cdot\vec{n}_s dl dy, \tag{30}$$

where y is the signed distance between a point of the side surface and the physical surface (and plays the same role as d) and dl is the increment of arclength along the contour C, which is defined by the intersection of the physical surface and the surface of the pillbox. We now evaluate this integral

for the first two terms of the stress tensor, as given by Eq. (16),

$$\oint_C \int_{-h}^{+h} \varepsilon^2 {U_y}^2 [-\vec{n}\otimes\vec{\Xi} - \Gamma\mathbf{I}]\cdot\vec{n}_s dl dy = \int_{-\infty}^{+\infty} \varepsilon {U_{0,z}}^2 dz \oint_C [-\vec{n}\otimes\vec{\Xi} - \Gamma\mathbf{I}]\cdot\vec{n}_s dl = \frac{4}{3}\varepsilon \oint_C [-\vec{n}\otimes\vec{\Xi} - \Gamma\mathbf{I}]\cdot\vec{n}_s dl. \tag{31}$$

By application of the surface divergence [4,52,58], we have

$$\oint_C [-\vec{n}\otimes\vec{\Xi}]\cdot\vec{n}_s dl = \int_S \vec{\nabla}_S\cdot[-\vec{n}\otimes\vec{\Xi}]dS - \int_S [-\vec{n}\otimes\vec{\Xi}]\cdot K\vec{n} dS \tag{32}$$

with $K = \vec{\nabla}_S\cdot\vec{n}$. Moreover, by definition of the vector $\vec{\Xi}$, we have $[-\vec{n}\otimes\vec{\Xi}]\cdot\vec{n} = -(\vec{\Xi}\cdot\vec{n})\vec{n} = \Gamma\vec{n}$. Similarly,

$$-\oint_C \Gamma\mathbf{I}\cdot\vec{n}_s dl = -\int_S \vec{\nabla}_S\Gamma dS + \int_S \Gamma K\vec{n} dS, \tag{33}$$

where $\vec{\nabla}_S\Gamma$ is the surface gradient of Γ. Then we use the identity $\vec{\nabla}\cdot(\vec{u}\otimes\vec{v}) = (\vec{\nabla}\vec{u})\cdot\vec{v} + (\vec{\nabla}\cdot\vec{v})\vec{u}$ and applied it to $-\vec{n}\otimes\vec{\Xi}$:

$$\vec{\nabla}_S\cdot(-\vec{n}\otimes\vec{\Xi}) = -\vec{n}\vec{\nabla}_S\cdot\vec{\Xi} - \mathbf{L}\cdot\vec{\Xi}, \tag{34}$$

where $\mathbf{L} = \vec{\nabla}_S\vec{n}$ is the curvature tensor [4], the opposite signs in the expressions for both K and $\mathbf{L}$, as compared to classical ones, comes from the definition of the normal vector in our model, which points toward Ω_+. Thus, we obtain

$$\oint_C \int_{-h}^{+h} \varepsilon^2 {U_y}^2 [-\vec{n}\otimes\vec{\Xi} - \Gamma\mathbf{I}]\cdot\vec{n}_s dl dy = \frac{4}{3}\varepsilon \int_S (-\vec{n}\vec{\nabla}_S\cdot\vec{\Xi} - \mathbf{L}\cdot\vec{\Xi} - \vec{\nabla}_S\Gamma) dS. \tag{35}$$

Then, we evaluate the contribution of the third term of the stress tensor [Eq. (16)] in the integral defined by Eq. (30). At leading order in ε, we find

$$\frac{\alpha^2}{2\varepsilon^2}W^2 = \frac{\alpha^2}{2}{W_1}^2 = \frac{\alpha^2}{2}K^2{U_{0,z}}^2, \tag{36}$$

and we are now able to calculate the following integral:

$$-\oint_C \int_{-h}^{+h} \frac{\alpha^2}{2\varepsilon^2}W^2\mathbf{I}\cdot\vec{n}_s dl dy = -\frac{\alpha^2}{2}\int_{-\infty}^{+\infty} \varepsilon {U_{0,z}}^2 dz \oint_C K^2\vec{n}_s dl = -\frac{2}{3}\varepsilon\alpha^2 \oint_C K^2\vec{n}_s dl. \tag{37}$$

The surface divergence theorem gives

$$\oint_C K^2\,\vec{n}_s dl = \int_S \vec{\nabla}_S K^2 dS - \int_S K^3\vec{n} dS, \tag{38}$$

and, therefore, Eq. (37) can be written, at leading order in ε, as

$$\frac{2}{3}\varepsilon\alpha^2 \int_S (K^3\vec{n} - \vec{\nabla}_S K^2) dS. \tag{39}$$

Now we evaluate the next term of the stress tensor, $\vec{\nabla}u\otimes\vec{\nabla}w$, and find

$$\vec{\nabla}u\otimes\vec{\nabla}w = \left(\vec{\nabla}_x U + \frac{1}{\varepsilon}U_z\vec{n}\right)\otimes\left(\vec{\nabla}_x W + \frac{1}{\varepsilon}W_z\vec{n}\right) = -{U_{0,z}}^2\vec{n}\otimes\vec{\nabla}_S K + \frac{1}{\varepsilon^2}W_z U_z\vec{n}\otimes\vec{n}, \tag{40}$$

where we have used that $\vec{\nabla}_x U_0 = 0$ and $\vec{\nabla}_x K = \vec{\nabla}_S K$ at leading order [42,59]. The term in $\vec{n}\otimes\vec{n}$ does not contribute to the integral, Eq. (30), since $(\vec{n}\otimes\vec{n})\cdot\vec{n}_s = (\vec{n}\cdot\vec{n}_s)\vec{n} = 0$. Therefore, we have

$$-\oint_C \int_{-h}^{+h} \alpha^2 {U_{0,z}}^2 [\vec{n}\otimes\vec{\nabla}_S K]\cdot\vec{n}_s dl dy = -\frac{4}{3}\varepsilon\alpha^2 \oint_C [\vec{n}\otimes\vec{\nabla}_S K]\cdot\vec{n}_s dl. \tag{41}$$

Still in applying the surface divergence theorem, we obtain

$$\oint_C [\vec{n}\otimes\vec{\nabla}_S K]\cdot\vec{n}_s dl = \int_S \vec{\nabla}_S\cdot[\vec{n}\otimes\vec{\nabla}_S K] dS - \int_S [\vec{n}\otimes\vec{\nabla}_S K]\cdot K\vec{n} dS = \int_S [\vec{n}\vec{\nabla}_S\cdot\vec{\nabla}_S K + \mathbf{L}\cdot\vec{\nabla}_S K] dS - \int_S [\vec{n}\cdot\vec{\nabla}_S K]\vec{n} K dS. \tag{42}$$

The last term of the right-hand side vanishes since, by definition, the surface gradient of any quantity is perpendicular to the normal vector. Thus, we obtain

$$-\oint_C \int_{-h}^{+h} \alpha^2 {U_{0,z}}^2 [\vec{n}\otimes\vec{\nabla}_S K]\cdot\vec{n}_s dl dy = -\frac{4}{3}\varepsilon\alpha^2 \int_S [\vec{n}\Delta_S K + \mathbf{L}\cdot\vec{\nabla}_S K] dS. \tag{43}$$

Finally, we evaluate the last term of the stress tensor, in $w\vec{\nabla}\vec{\nabla}u$, and we find at leading order,

$$w\vec{\nabla}\vec{\nabla}u = -K{U_{0,z}}^2\vec{\nabla}_x\vec{n} - \frac{K}{\varepsilon}U_{0,z}U_{0,zz}\vec{n}\otimes\vec{n}, \tag{44}$$

where we have used $\vec{\nabla}_x U_{0,z} = 0$. Once again, the term in $\vec{n}\otimes\vec{n}$ does not contribute to the integral, Eq. (30), since $(\vec{n}\otimes\vec{n})\cdot\vec{n}_s = 0$. Moreover, as $\vec{\nabla}_x\vec{n} = \vec{\nabla}_S\vec{n} = \mathbf{L}$ at leading order, we have

$$-\oint_C \int_{-h}^{+h} \alpha^2\left(-K{U_{0,z}}^2\mathbf{L}\right)\cdot\vec{n}_s dl dy = \frac{4}{3}\varepsilon\alpha^2 \int_S [K\vec{\nabla}_S\cdot\mathbf{L} + \mathbf{L}\cdot\vec{\nabla}_S K - K^2\mathbf{L}\cdot\vec{n}] dS. \tag{45}$$

Since the curvature tensor is tangential, $\mathbf{L}\cdot\vec{n} = 0$ (and $\mathbf{L} = \mathbf{L}_{\text{Tan}}$, its tangential component) [4]. Moreover, $\vec{\nabla}_S\cdot\mathbf{L} = \vec{\nabla}_S K - |\mathbf{L}|^2\vec{n}$ [4]. Considering that the surface of integration S is arbitrary, the equilibrium condition $\vec{\nabla}.\,\mathbf{S} = 0$ is derived from Eq. (35), Eq. (39), Eq. (43), and Eq. (45), projected on $\vec{n}$:

$$-\vec{\nabla}_S\cdot\vec{\Xi} - \alpha^2\left(\Delta_S K + K|\mathbf{L}|^2 - \frac{K^3}{2}\right) = 0, \tag{46}$$

since $\vec{\nabla}_S\Gamma$, $\vec{\nabla}_S K$, and $\vec{\nabla}_S K^2$ are tangent to the physical surface. We have also used the fact that $\mathbf{L}\cdot\vec{\Xi}$, with $\vec{\Xi} = -\Gamma(\vec{n})\vec{n} - \mathbf{P}\cdot\vec{\nabla}_n\Gamma(\vec{n})$, is tangent to the surface. Indeed, $\mathbf{L}\cdot\vec{\Xi} = -\mathbf{L}\cdot(\mathbf{P}\cdot\vec{\nabla}_n\Gamma) = -\mathbf{L}\cdot\vec{\nabla}_n\Gamma$ since $\mathbf{L}\cdot\vec{n}$ and $\mathbf{L}\cdot(\vec{n}\otimes\vec{n}\cdot\vec{\nabla}_n\Gamma) = (\vec{n}\cdot\vec{\nabla}_n\Gamma)\mathbf{L}\cdot\vec{n} = 0$. As the curvature tensor is tangential, one can show that $\mathbf{P}\cdot\mathbf{L}\cdot\mathbf{P} = \mathbf{L}_{\text{Tan}} = \mathbf{L}$ [4]. It follows that $\mathbf{L}\cdot\vec{\Xi} = \mathbf{P}\cdot(\mathbf{L}\cdot\vec{\Xi})$, the projection of the vector $\mathbf{L}\cdot\vec{\Xi}$ onto the physical surface returns the vector, i.e., the latter is tangent to the surface.

Furthermore, it can be shown that $\Delta_S K + K|\mathbf{L}|^2 - \frac{K^3}{2} = \Delta_S K - 2KG + \frac{K^3}{2}$ [14]. Therefore,

$$-\vec{\nabla}_S\cdot\vec{\Xi} - \alpha^2\left(\Delta_S K - 2KG + \frac{K^3}{2}\right) = 0. \tag{47}$$

The above equilibrium condition is the main result of this work. It shows that the phase-field model converges formally toward the regularized sharp-interface theory [Eq. (5)], in the limit $\varepsilon \ll \alpha$. In two dimensions we have shown that, in the limit $\varepsilon \ll \alpha$, the normal interfacial velocity v_n is proportional to the energy difference between the flat and curved surfaces and converges to the sharp-interface result for motion-by-curvature [48],

$$v_n = \hat{\Gamma}(\theta)\kappa - \alpha^2\left(\kappa_{ss} + \frac{\kappa^3}{2}\right), \tag{48}$$

where $\hat{\Gamma}(\theta) = \Gamma(\theta) + \Gamma_{\theta\theta}(\theta)$ is the dimensionless interface stiffness and θ the surface orientation (measured anticlockwise from a fixed direction). $\Gamma(\theta)$ is the dimensionless surface energy, κ is the interface curvature, and s the arclength. In the direction of increasing s the region Ω_+ is on the right. In two dimensions, $-\vec{\nabla}_S\cdot\vec{\Xi} = \hat{\Gamma}\kappa$ with negative $\kappa = \theta_s$ when Ω_+ forms a bump. Assuming that, in three dimensions, the interfacial velocity remains proportional to the energy difference between the flat and curved surfaces [Eq. (47)], extension of Eq. (48) gives:

$$v_n = -\vec{\nabla}_S\cdot\vec{\Xi} - \alpha^2\left(\Delta_S K - 2KG + \frac{K^3}{2}\right), \tag{49}$$

which is the dimensionless form of the sharp-interface velocity for regularized anisotropic motion-by-curvature [Eq. (4)]. In the present analysis, we have formally demonstrated, in the limit $\varepsilon \ll \alpha$, the convergence of the phase-field model toward the sharp-interface equilibrium condition in three dimensions [Eq. (5)]. As mentioned earlier, in the dynamic settings, we had previously shown that the model converges toward the sharp-interface theory for anisotropic motion-by-curvature in two dimensions [48]. Moreover, in three dimensions, the regularized but isotropic model was shown to converge toward motion-by-curvature by Loreti and March [42]. Therefore, in light of the present analysis, it is reasonable to consider that the phase-field model mimics anisotropic motion-by-curvature in three dimensions, despite the fact that its formal convergence toward Eq. (49) is not yet proved. In the other limit, $\alpha < \varepsilon$, the presence of corners with high curvatures (small corner size) is expected to modify the *tanh* profile for the phase-field u in the corner region. In turn, both the equilibrium condition and the normal velocity may deviate from the sharp-interface results. Corners, in this limit, were studied in two dimensions [56] and, indeed, we found that the model does not converge toward sharp-interface theory; however, the phase transition at the interface is preserved and presents the same properties as the classical problem. Therefore, the model can also be used in the limit of small corner size, as compared with interface thickness, since regularization still operates. However, asymptotic convergence toward sharp-interface corners is lost. Now that we have discussed the convergence of the phase-field model toward the sharp-interface theory, we investigate, in the next section, the effect of the regularization parameter on corner's morphology at equilibrium.

III. CORNERS

In the nonregularized sharp-interface picture, Cahn and Hoffman have shown that [16]

$$-\vec{\nabla}_S\cdot\vec{\Xi} = \mu \tag{50}$$

at equilibrium, where μ is the dimensionless free-energy difference between the two coexisting phases. The simplest solution to the above equation arises for an isolated particle such that its radius vector from the origin to a point of the particle surface satisfies [16]:

$$\vec{r} = -\frac{2}{\mu}\vec{\Xi}. \tag{51}$$

Since $\vec{\nabla}_S\cdot\vec{r} = 2$, the equilibrium condition is thereby satisfied. Therefore, the equilibrium shape is geometrically similar to the $\vec{\Xi}$ plot [16] and inversely proportional to μ. Using the spherical polar angles θ and φ, the $\vec{\Xi}$ vector is given by $\vec{\Xi} = \Gamma\vec{e}_r + \Gamma_\theta\vec{e}_\theta + \Gamma_\varphi\vec{e}_\varphi/\sin\theta$, where $\vec{e}_r = -\vec{n}$, with our definition of the normal vector. Converting to Cartesian coordinates (x, y, z) yields:

$$x = \Gamma\sin\theta\cos\varphi + \Gamma_\theta\cos\theta\cos\varphi - \Gamma_\varphi\sin\varphi/\sin\theta, \tag{52}$$

$$y = \Gamma\sin\theta\sin\varphi + \Gamma_\theta\cos\theta\sin\varphi + \Gamma_\varphi\cos\varphi/\sin\theta, \tag{53}$$

$$z = \Gamma\cos\theta - \Gamma_\theta\sin\theta. \tag{54}$$

As an illustration, the $\vec{\Xi}$ plot is shown in Fig. 2 for the following anisotropy function:

$$\Gamma(\vec{n}) = 1 + p\left(4\sum_{i=x,y,z} {n_i}^4 - 3\right) \tag{55}$$

for $p = 0.05$ [Fig. 2(a)]. One can see that the equilibrium shape is nonspherical but it remains smooth. The regions of high curvature correspond to directions of high surface energies. When p is further increased the surface energy is strongly anisotropic and nonconvex, "ears" appear on the $\vec{\Xi}$ plot. Some orientations are missing on the equilibrium shape, which now presents sharp corners and edges [Fig. 2(b), $p = 0.15$]. For $p = 0.15$, four orientations coexist at equilibrium in the corner region (four-face pyramids). For $p = -0.15$ the Γ

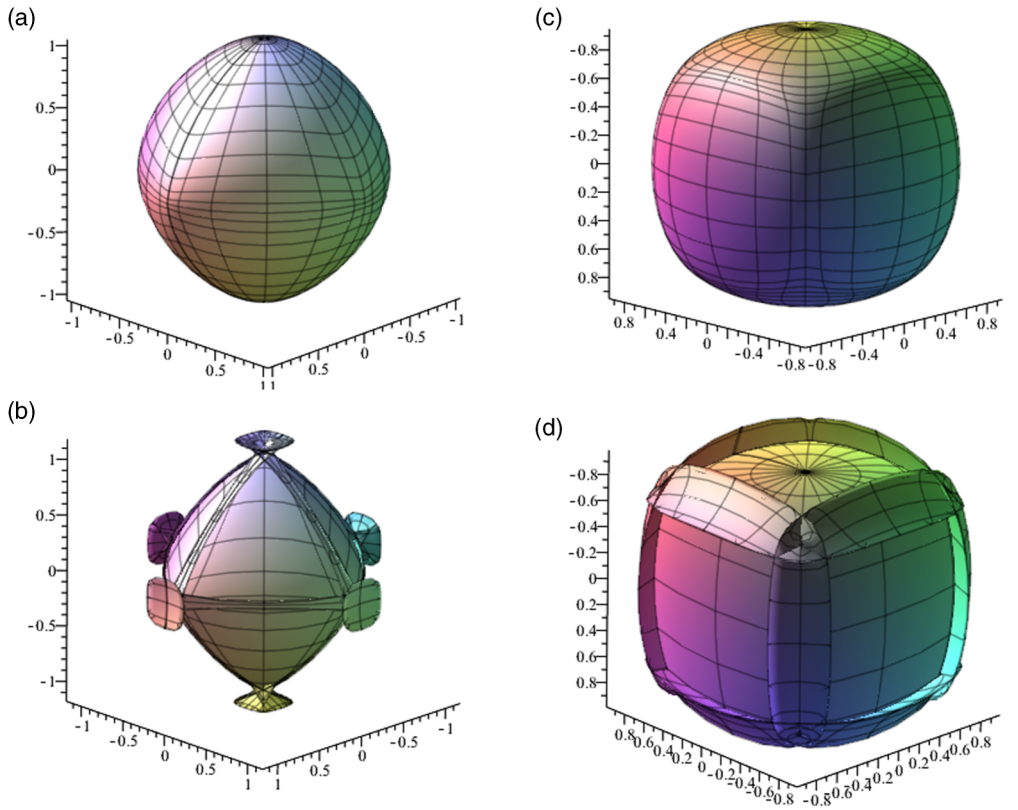

FIG. 2. The $\vec{\Xi}$ plot for $\Gamma = 1 + p(4\sum_{i=x,y,z} n_i{}^4 - 3)$ with $p = 0.05$ (a) and $p = 0.15$ (b). The orientations for which the $\vec{\Xi}$ vectors form the exterior flaps and ears of the $\vec{\Xi}$ plot (b) are excluded from the equilibrium shape. These are the so-called missing orientations. (c) The $\vec{\Xi}$ plot for $p = -0.05$. (d) The $\vec{\Xi}$ plot for $p = -0.15$.

function presents trigonal symmetry, three orientations coexist at the corner [Fig. 2(d)]. In three dimensions, the criterion for the onset of missing orientations has been derived by Sekerka [60]. In two dimensions, Γ reduces to $\Gamma = 1 + p\cos 4\theta$ with θ the surface orientation. Corners are visible on the equilibrium shape when the surface stiffness, $\hat{\Gamma}(\theta) = \Gamma(\theta) + \Gamma_{\theta\theta}(\theta)$, is negative for some orientations, i.e., when $p \geqslant 1/15$.

For a sufficiently large value of the parameter p, say, $p = 0.5$, corners in the sharp-interface theory are sharp [as in Fig. 2(b)]. In the present phase-field model, corners are rounded since regularization penalizes the interfacial regions of high curvatures. In the energy [Eq. (7)], the bending length α prescribes the corner size. Let us examine the effect of regularization on the morphology of the corners in the phase-field model. In the phase-field simulations, for which periodic boundary conditions are used, the initial configuration is prepared such as a corner is present, of random size and shape, and the system relaxes toward equilibrium [via the Allen-Cahn equation, Eq. (11)]. The interface width ε is 0.2 and the cubic anisotropy function [Eq. (55)] is used for $p = 0.5$. Corners are shown in Fig. 3 for configurations near equilibrium. The isosurface of the phase field $u = 0$ is shown for two corner sizes $\alpha = 0.2$ and $\alpha = 0.5$. As expected, corners size scales in α. For $\alpha > \varepsilon$ corners formally satisfy Eq. (47). For $\alpha = \varepsilon$ the shape of corners resembles sharp-interface corners even if the strict convergence is lost [56]. To our knowledge, the analytical solution for a regularized corner at equilibrium [solution of Eq. (47)] is not known in the sharp-interface problem in three dimensions. The two-dimensional problem has been solved by Spencer [13]. However, in three dimensions, it is possible to derive the far-field solutions when a small slope approximation is employed [17]. We will make this assumption in order to derive the far-field solution for a corner at equilibrium and compare it to simulations. In the sharp-interface model, the total dimensionless energy of a surface S is

$$E = \int_S \Gamma^* \sqrt{1 + |\vec{\nabla} h|^2}\, dx dy, \tag{56}$$

where $h(x, y)$ gives the surface location, and $\Gamma^* = \Gamma(\vec{n}) + \alpha^2 K^2/2$ is the dimensionless regularized surface energy with as before α the corner size and K the total curvature of the interface. We then employ the small slope approximation $|h_x| \ll 1$ and $|h_y| \ll 1$ and expand the weighted surface energy $\Gamma^* \sqrt{1 + |\vec{\nabla} h|^2}$:

$$\begin{aligned} &\Gamma^* \sqrt{1 + |\vec{\nabla} h|^2} \\ &\quad \sim \varepsilon_0 + \varepsilon_1 ({h_x}^2 + {h_y}^2) + \varepsilon_2 \left({h_x}^4 + {h_y}^4\right) \\ &\qquad + \varepsilon_3 \left({h_x}^2 {h_y}^2\right) + \cdots + \frac{\alpha^2}{2} ({h_{xx}}^2 + 2 h_{xx} h_{yy} + {h_{yy}}^2) \end{aligned} \tag{57}$$

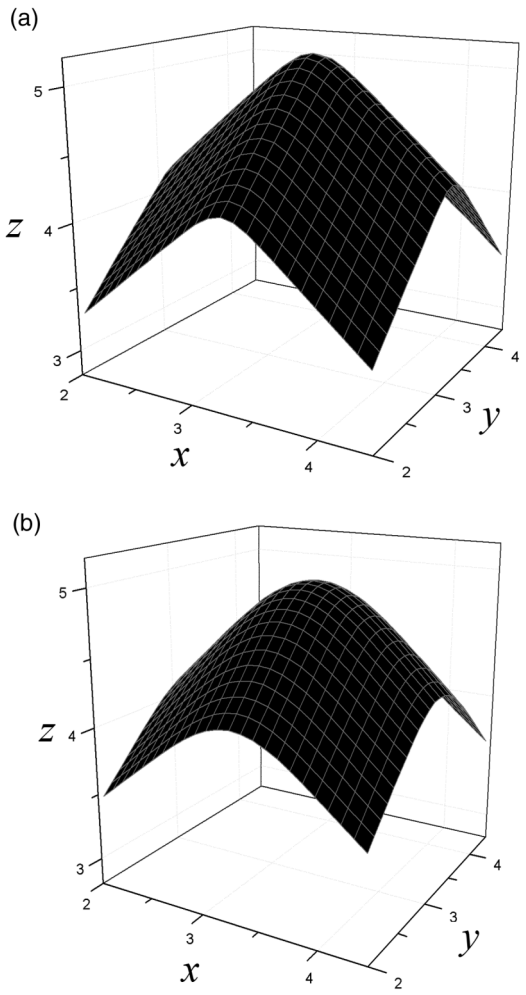

FIG. 3. Corners near equilibrium (as defined by the isosurface $u = 0$) for the anisotropic surface energy Γ of Eq. (55) with $p = 0.5$ and for two corner sizes $\alpha = 0.2$ (a) and $\alpha = 0.5$ (b).

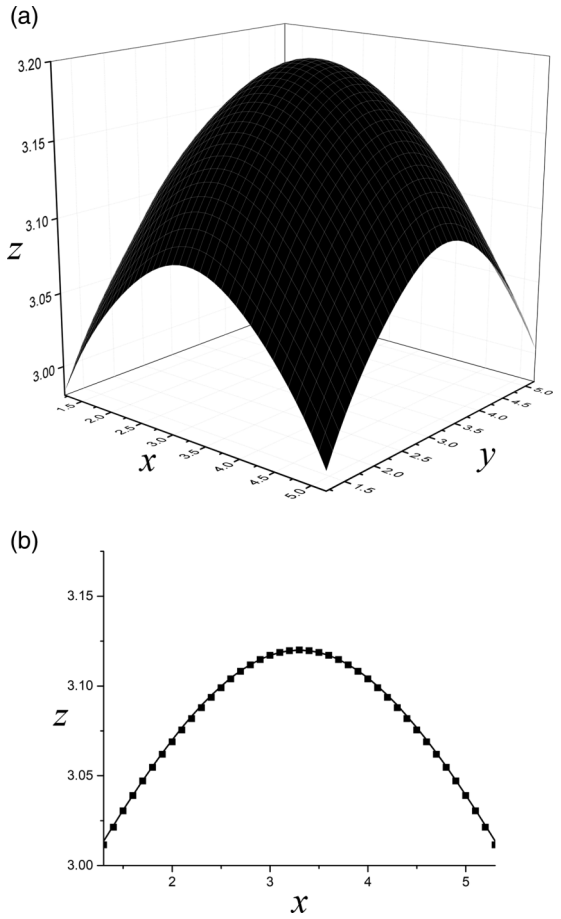

FIG. 4. (a) A corner near equilibrium (as defined by the isosurface $u = 0$) for the anisotropic surface energy Γ of Eq. (55) with $p = 0.07$. (b) The phase-field profile (black squares) along an edge far from the corner is compared to the analytical far-field solution in the small slope approximation (solid line). For clarity, the z axis is stretched as the far-field slope is small ∼0.1.

with $\varepsilon_0 = 1 + p$, $\varepsilon_1 = 1/2 - 15p/2$, $\varepsilon_2 = -1/8 + 95p/8$, and $\varepsilon_3 = -1/4 + 63p/4$ for the cubic surface energy Γ defined by Eq. (55). At equilibrium, the Euler-Lagrange condition $\delta E/\delta h = 0$ up to fourth order leads to a nonlinear partial differential equation for the crystal shape [17]:

$$-m\vec{\nabla}^2 h + \left(a{h_x}^2 + b{h_y}^2\right)h_{xx} + \left(b{h_x}^2 + a{h_y}^2\right)h_{yy} + c h_x h_y h_{xy} - \alpha^2\vec{\nabla}^4 h = 0, \quad (58)$$

where $m = -2\varepsilon_1$, $a = 12\varepsilon_2$, $b = 2\varepsilon_3$, and $c = 8\varepsilon_3$. We can now determine the far-field solution. As in Golovin *et al.* [17], the solution along an edge is supposed to have the following asymptotic behavior:

$$h \sim Ay + f(x), \quad (59)$$

as $y \to -\infty$. A is the far-field slope and $f(x)$ a function to be determined. For $x \to -\infty$, we have $h \sim Ax + f(y)$. This implies $f'(\pm\infty) = \mp A$. Taking the ansatz $f' = Q\tanh kx$, and substituting into the equilibrium condition yields $Q^2 = 3(m - bA^2)/a$ and $k^2 = aQ^2/6\alpha^2$. As $Q^2 = A^2$ (compatibility condition), we have for the far-field slope:

$$A = \sqrt{\frac{3m}{a + 3b}}. \quad (60)$$

This allows us to determine the crystal shape for $y \to -\infty$:

$$h \sim Ay - \sqrt{\frac{6\alpha^2}{a}}\ln\left[\cosh\left(\sqrt{\frac{a}{6\alpha^2}}Ax\right)\right]. \quad (61)$$

This coincides with the solution derived in Ref. [14], but the coefficients are quantitatively different in our analysis as we use another function for the anisotropic surface energy. We can now compare this solution along an edge to phase-field simulations for a corner at equilibrium (Fig. 4). The phase-field profile (defined by the isosurface $u = 0$) along an edge and the analytical solution in the small slope approximation are shown Fig. 4(b). This comparison is made for $p = 0.07$, and $\alpha = \varepsilon = 0.2$. The agreement is very good. Here we restrict ourselves to low values of p. In practice, we find that the far-field slopes A, in the small slopes approximation, may rapidly depart from their expected thermodynamic values

[13], as given by the common tangent construction for the weighted surface energy, as soon as $p > 0.1$.

IV. PHASE SEPARATION OF CRYSTAL SURFACES

In this section, we apply the regularized phase-field model to the interfacial phase separation. As it is well known, a crystal surface will phase separate if its orientation is a missing orientation. In two dimensions, there is an analytical criteria, missing orientations intervene as soon as the stiffness $(\Gamma + \Gamma_{\theta\theta})$ is negative for some orientations. The equivalent analytical criteria in three dimensions was recently formulated by Sekerka [60] and used in the following to determine the presence of the missing orientations, and, therefore, the presence of the interfacial phase separation. In this case, the surface may be metastable, which corresponds to the nucleation regime, or unstable. The latter regime is known as the spinodal of facets, and unstable interfaces will decompose into stable facets [7]. This instability is also known as the faceting instability or as the Herring instability. The thermodynamics origin of this process is theoretically well understood. The analogy with spinodal decomposition is often made as the phase separation is similar to spinodal decomposition in alloys since the role played by the surface orientation is close to that of composition in alloys.

A. Faceting instability

The spinodal decomposition of a thermodynamically unstable surface into facets has been commonly observed in metals, ceramics, and semiconductors [61–65]. In principle, stepped surfaces, i.e., a misoriented singular surfaces (or facets) may also phase separate. Thermodynamics predicts the nature of the stable surfaces resulting from the decomposition of a stepped surface, which may be either facets (singular surfaces) or a mixture of facets and rough surfaces [41]. However, more complex interactions are responsible for phase separation between a facet and a stepped surface or between two surfaces of different stepped density, as for the reconstruction of a misoriented Si(111) surface [41,65]. There are many areas where the interfacial phase separation is at stake. For example, the phase separation at the interface has been evidenced during thermal grain boundary grooving [66,67] with grooving profiles of tungsten in vacuum exhibiting a faceted morphology at high temperature. Moreover, grain boundaries may also facet [68]. The latter example also underlines the importance of elastic effects on the faceting kinetics of some surfaces [37]. In fact, Stewart and Goldenfield [19] have shown, following Marchenko's work [69], that the interface stress may alter the dynamics of spinodal decomposition of a crystal surface at long times. Elastic effects are ignored in the present approach since our aim is to illustrate the interfacial phase separation with the classical motion-by-curvature kinetics [Eq. (4)] that does not contain the elastic contribution. Let us mention another type of surface for which the interfacial phase separation operates. Indeed, an initially stable surface may facet as oxygen exposure modifies the surface energy anisotropy [70,71]. This process is known as adsorbate-induced faceting and can be used as nanotemplates, for instance, to synthesize metallic nanoparticles [72]. This makes the faceting problem of practical interest also. In our paper, when we refer to the faceting instability, it means that an unstable surface will decompose into stable surfaces, but such surfaces are rough as the surface energy is differentiable in our model. We may also refer to facets in the following when describing the nearly faceted morphology, but it shall be kept in mind that it is a misnomer.

We first investigate the dynamics of the faceting instability in the context of pure motion-by-curvature for crystal surfaces with trigonal symmetry leading to the formation of triangular pyramids. The dissipative evolution equation (i.e., the Allen-Cahn equation in phase-field theory) mimics attachment-kinetics limited growth. Trigonal symmetry is reproduced for negative p in the Γ function given by Eq. (55), see Fig. 2(c) and Fig. 2(d). We set $p = -0.7$ in the following and study the faceting instability around one of the four corners of the Wulff plot [Fig. 2(d)] as they are all identical. At $t = 0$ the initial flat surface is randomly perturbed so that to initiate the decomposition with fluctuations of all possible wavelengths. Phase separation will then lead to the formation of triangular pyramids of which orientations correspond to that of the three stable surfaces near the corner of the Wulff shape [Fig. 2(d)]. Figure 5 shows two snapshots of the simulation at different times. The top views shows the crystalline surface as defined by the isosurface of the phase field ($u = 0$). In the simulations we have used $\varepsilon = 0.1$ and $\alpha = 0.2$, as well as periodic boundary conditions. As expected, the surface is made of triangular pyramids. In this illustration, the facets have the same surface energy, the only way for the system to decrease its energy is to decrease the length of the network made by corners and edges. The bending energy is the driving force for the coarsening process, and concomitantly the mean facet size increases and the number of pyramids decreases. We define the following characteristic morphological length scale L, as $(L_x + L_y)/2$ with L_x and L_y the mean distances between corners (or edges) in, respectively, the x and y directions. L is plotted versus time t in Fig. 6. A $t^{1/3}$ scaling law is found after an initial transient, as predicted by sharp-interface theory and simulations [25]. The topological events that we observe are identical to that found by Watson and Norris in the sharp-interface formulation [25], see Fig. 7, coarsening proceeds by edge contraction, which leads to the disappearing of one facet as the two adjacent facets merge, or by cube removal, for which the three facets simultaneously disappear to form one corner.

The exponent 1/3 was also found in the coarsening dynamics of triangular pyramids [73,74] resulting from the Ehrlich-Schwoebel instability [75,76]. This is not surprising as the free-energy formulation of the continuum model resembles Eq. (56). It involves a potential that favors particular orientations (the so-called magic slopes) of the pyramid surfaces and that is regularized with a bending energy. The dynamics is also of type-A, as for thermodynamic faceting kinetically controlled by the condensation-evaporation mechanism, i.e., by motion-by-curvature. Therefore, the present phase-field model is a suitable formulation of this sharp-interface problem also.

Coarsening of triangular pyramids (e.g., 111 surfaces, trigonal symmetry) was also investigated by Golovin *et al.* [17] in the sharp-interface model, also with type-A dynamics, and

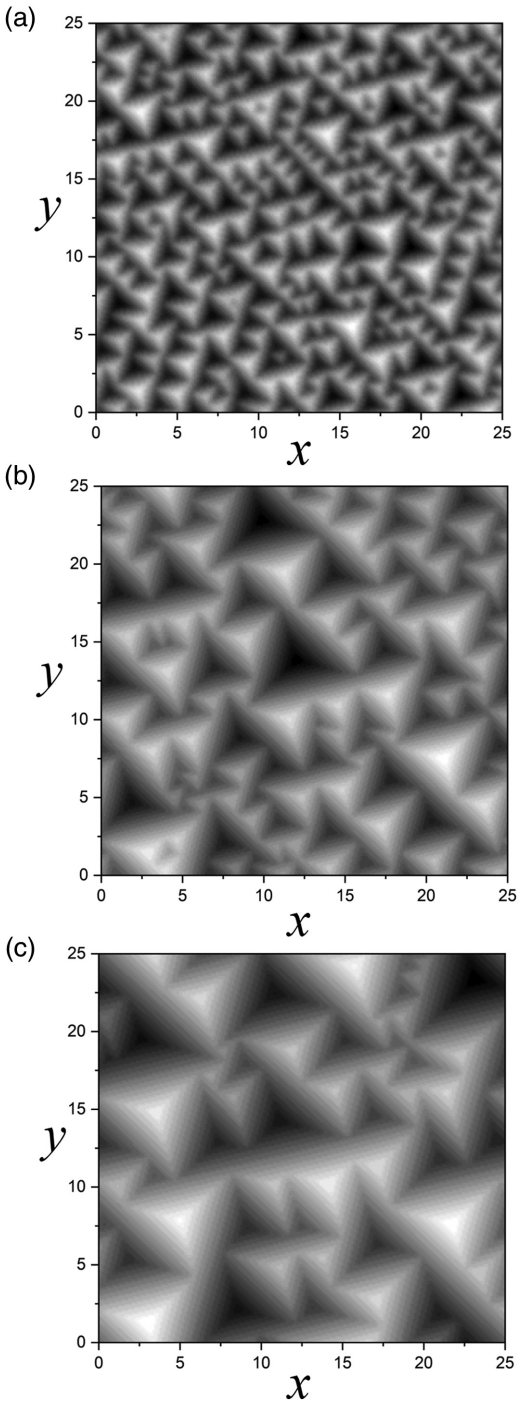

FIG. 5. (a) Top view of the crystal surface at $t = 0.8$ (as defined by the isosurface $u = 0$) for the anisotropic surface energy Γ of Eq. (55) with $p = -0.7$. In the simulation, we have used $\varepsilon = 0.1$ and $\alpha = 0.2$. (b) Top view of the crystal surface at $t = 10$ and (c) at $t = 50$. The gray scale gives the height of the surface.

in the small slope approximation. Their numerical simulations give a coarsening exponent close to $1/2$. They also observed a value close to $1/2$ for square pyramids (e.g., 001 surfaces, quadratic symmetry). This is close to the theoretical prediction $(1/2)$ made by Mullins [77] when dynamics of surface reconstruction is governed by the condensation-evaporation mechanism, but considerably larger than that

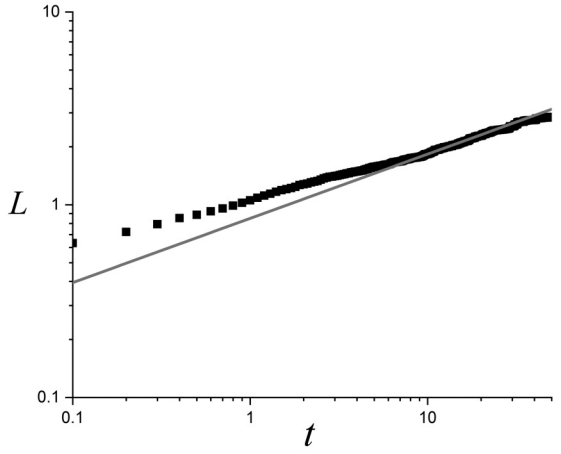

FIG. 6. Characteristic domain size L versus time t measured in the phase-field simulation during coarsening of triangular pyramids (black squares). The solid gray line shows a $\sim t^{1/3}$ trend for sake of comparison. L is defined as $(L_x + L_y)/2$ with L_x and L_y the mean distances between corners (or edges) in, respectively, the x and y directions.

obtained by direct power counting in the motion equation, which predicts the estimate $1/4$ [18,78]. In any case, coarsening is faster in Golovin's study [17] as his model includes a driving force for growth and therefore convective effects are present, which are known to contribute to fast coarsening [11,12,20,48]. The coarsening dynamics of square pyramids was also thoroughly studied by Moldovan and Golubovic [74], if most realizations can be described by an exponent $1/4$, as also observed by Siegert [73] and Liu and Metiu [18], it presents in reality a more subtle behavior, see Ref. [74] for more details.

B. Nucleation of crystal surfaces

Another interesting problem that may be addressed with the present phase-field model is nucleation of crystal surfaces. This time, the initial orientation of the surface is metastable, which implies for the system to overcome a nucleation barrier before entering into the growth regime (for the new formed facet). We will investigate the early stages of this interfacial phase separation in the nucleation-growth regime. We are aware of only a few theoretical studies on this phenomena [18,79], as most of the efforts were dedicated to understand the dynamics of spinodal of facets. Those studies were limited to two dimensions but the problem is fully three dimensional, even when the phase separation only presents two stable facets (such as terrace-and-step structures). Thus, in the present work, we study nucleation of crystal surfaces in three dimensions. We restrict ourselves to type-A dynamics (motion-by-curvature). For this purpose we now set $p = -0.5$ in the anisotropy function [Eq. (55)] and use $\varepsilon = 0.2$ and $\alpha = 0.2$ in our phase-field simulations with periodic boundary conditions. We choose the initial orientation around one of the edge regions of the Wulff plot [Fig. 2(d)] and in the metastable regime of the phase separation but close to the spinodal limit (i.e., low nucleation barrier). One has to introduce noise in the simulations to enhance nucleation of the stable orientation,

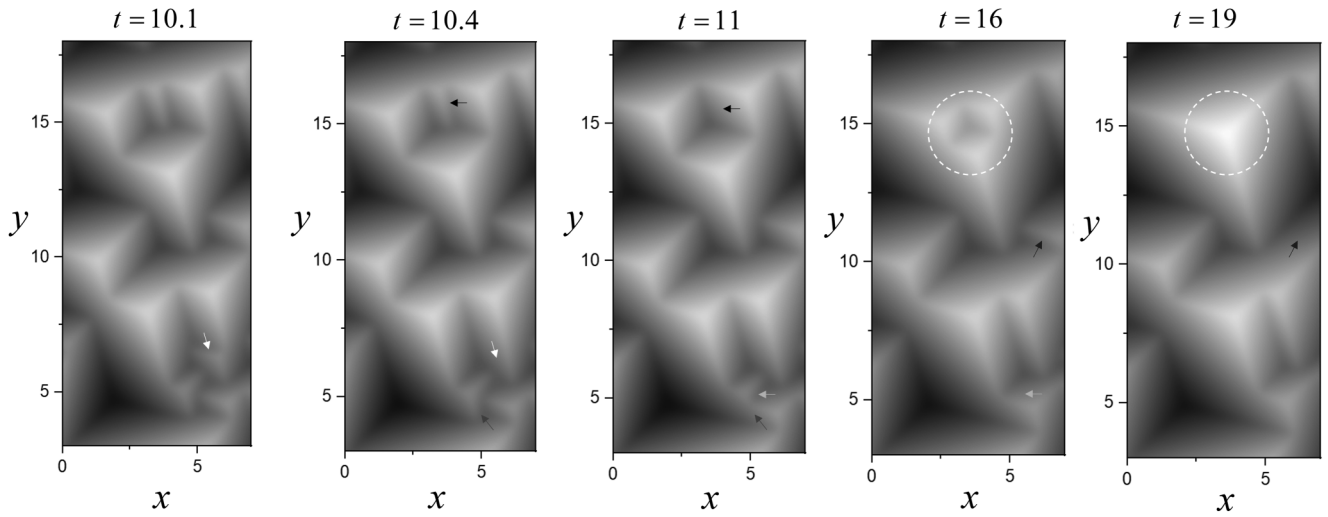

FIG. 7. Top view of the crystal surface at various times for a small region of the simulations shown in Fig. 5. Coarsening proceeds by edge contraction, which leads to the disappearing of one facet (marked by arrows on the figures) or by cube removal (dotted circle).

which is a thermally activated rare event. The noise is introduced in the same spirit than in the sharp-interface theory [21], and a term proportional to $AX\,p_u(u)$ is added to the Allen-Cahn equation [Eq. (11)] with $p(u) = (1+u)^2(2-u)/4$ and X is uniformly distributed on the interval $[-1, 1]$. The same value of X is used for all points in the direction normal to the interface. A is a constant, independent of time, that sets the amplitude of the noise and is related to temperature, but we are not interested here in a precise relationship between parameters and temperature. However, we need to work in the small noise regime in order for the calculation of critical shapes without noise to remain a good approximation [21]. According to the analysis performed in Ref. [48], the addition of such a term in the Allen-Cahn equation will modify the normal velocity of the interface with a term proportional to AX. In other words, noise is not added to the phase field u itself, as done in classical phase-field simulations with noise, but this is the interface location that is perturbed. Indeed, the model presents two types of phase transition involving the phase field u and also its gradient $\overrightarrow{\nabla} u$ (the interface orientation). The noise addition is designed to perturb $\overrightarrow{\nabla} u$, so that to initiate the corresponding interfacial phase transition. With our choice of parameters for the Γ function and the orientation of the initial surface, the final state is expected to be a "mixture" of two phases as there are two stable orientations, one of each side of the edge [Fig. 2(d)], which share a common direction, say, y. At long times, the system can be reduced to two dimensions (x, z), considering that the time needed for a facet to shrink in the parallel direction is negligible in front of the coarsening time. This is not true at the early stages since nucleation requires also growth of the newly formed facet in the y direction. The shape of the critical nucleus (the newly formed facet) is known for such a system, and must satisfy in two dimensions Eq. (48) for $v_n = 0$, since the critical shape corresponds to an unstable equilibrium, i.e., a saddle point [21]. The three-dimensional saddle-point solution is given by the 2D solution translated in the y direction, as this construction indeed satisfies Eq. (47).

The results of the phase-field simulations are given in Fig. 8, Fig. 9, and Fig. 10. Figure 8 shows the early stages of the nucleation process. The newly formed facets, resulting from thermal fluctuations, enter into the growth regime once they reach a given size (and shape). Those supercritical crystal surfaces are found to correspond to a local deformation of the initial surface, which indicates that ridge-crossing nucleation is dynamically favored. In the sharp-interface theory, it was shown by two-dimensional simulations of the equation of motion that ridge-crossing is preferred over saddle-point nucleation since the latter would require a nonlocal deformation of the initial surface [21]. We find that ridge crossing is also dynamically favored in our three-dimensional phase-field simulations. The phase-field simulations also show nucleation at random locations. Nucleation of crystal surfaces is known to present a very specific feature, called induced nucleation (or enhanced nucleation) [18,61,79,80], when a facet nucleates nearby a growing facet. Induced nucleation is expected to affect the dynamics of the phase separation, as compared to classical thermally activated nucleation. Furthermore, the induced facet shows characteristics that are different from that of the first critical facet. Nevertheless, such a process is not observed in our simulations where the dynamics is of type-A (condensation-evaporation). The induced nucleation mechanism, when a facet induces at its wake formation of additional facets, is therefore not evidenced in our phase-field simulations. Actually, the regions near the new facet are found to remain in the metastable regime and with a lower driving force as compared to that of the initial orientation of the crystalline surface. Therefore, nucleation near a facet is still possible but less probable. This suggests that induced nucleation is peculiar to the surface diffusion mechanism [18], as the formation of the first facet is very local in this regime and would lead to the appearance of unstable orientations in the regions adjacent to the newly formed facet, where one or more induced facets are then formed. Figure 9 shows that nucleation and growth of the formed facets lead to a two phases system, very similar to "step-and-terrace" surfaces. Concomitantly, some facets are found to shrink, and coarsening operates. As

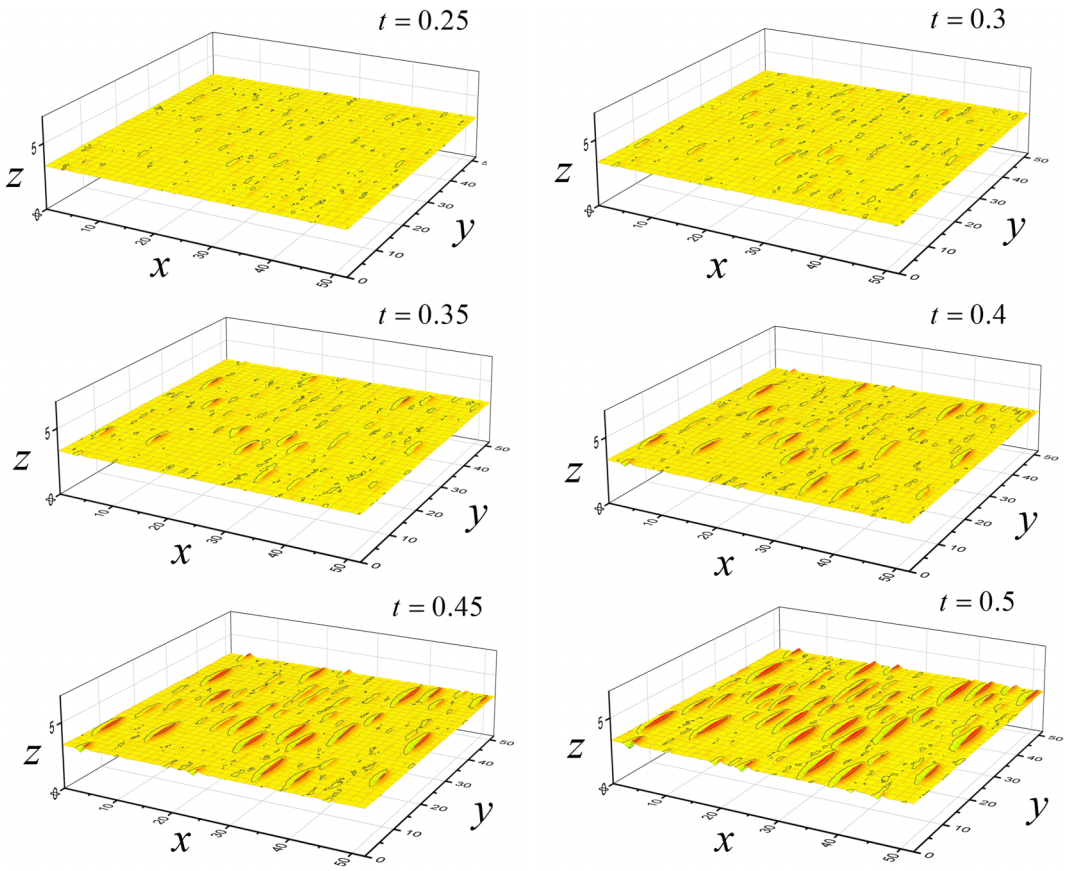

FIG. 8. Snapshots of the phase-field simulations during the first stages of nucleation of crystal surfaces at various times. Only the isosurfaces $u = 0$ are shown. For clarity, the z axis is stretched.

expected, the system reduces to two dimensions (x, z) at long times ($t \approx 20$), as the facets are infinite in the y direction (Fig. 10).

V. SUMMARY

From the divergence-free diffuse stress tensor, we have shown that the present phase-field model converges toward the equilibrium condition of the regularized sharp-interface theory in the limit of small interface thickness. In the dynamic setting, this result suggests the convergence of the Allen-Cahn version of the regularized phase-field model toward the sharp-interface theory for strongly anisotropic motion-by-curvature, even if the formal convergence remains to be established in three dimensions. We have also compared the shape of the corners at equilibrium, as given by the phase-field simulations, to theory, and we found a good agreement between simulations and theory for the far-field solutions in the small slope approximation. Then we have investigated the dynamics of the coarsening regime for crystal surfaces with trigonal symmetry resulting from the faceting instability, and we recovered the following scaling law $L \sim t^{1/3}$ for the growth in time t of a characteristic morphological length scale L. The topological events arising during coarsening were found to be identical to those of the sharp-interface problem. Finally, we have studied nucleation of crystal surfaces for a two-phase system. We found that ridge crossing is dynamically favored as nucleation operates via a local deformation of the initial surface. Moreover, we found no evidence of induced nucleation. This work demonstrates that the regularized phase-field model is a suitable formulation of the sharp-interface problem for phase separation of crystal surfaces. It could be used to study crystal surfaces with other symmetry, the influence of growth on the coarsening dynamics, as well as the effect of interface stress on the phase separation [19,37,69]. Therefore, the present phase-field model shall allow one to model faceting of realistic crystalline surfaces. Our generic model mimics pure motion-by-curvature, which can be applied and extended to many different interfaces and problems, such as

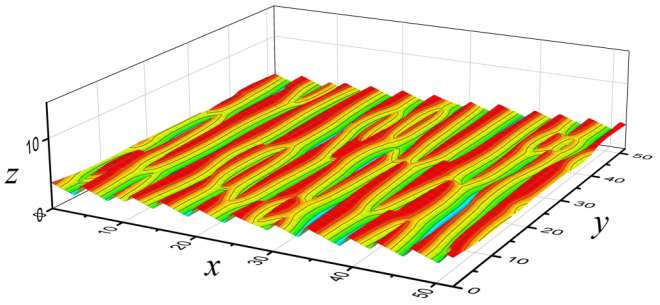

FIG. 9. The isosurface $u = 0$ at $t = 2$, as given by the phase-field simulation. The system is a "mixture of two phases" (or orientations) similar to "step-and-terrace" surfaces and resulting from nucleation and growth of crystal surfaces, which then enters into the coarsening regime.

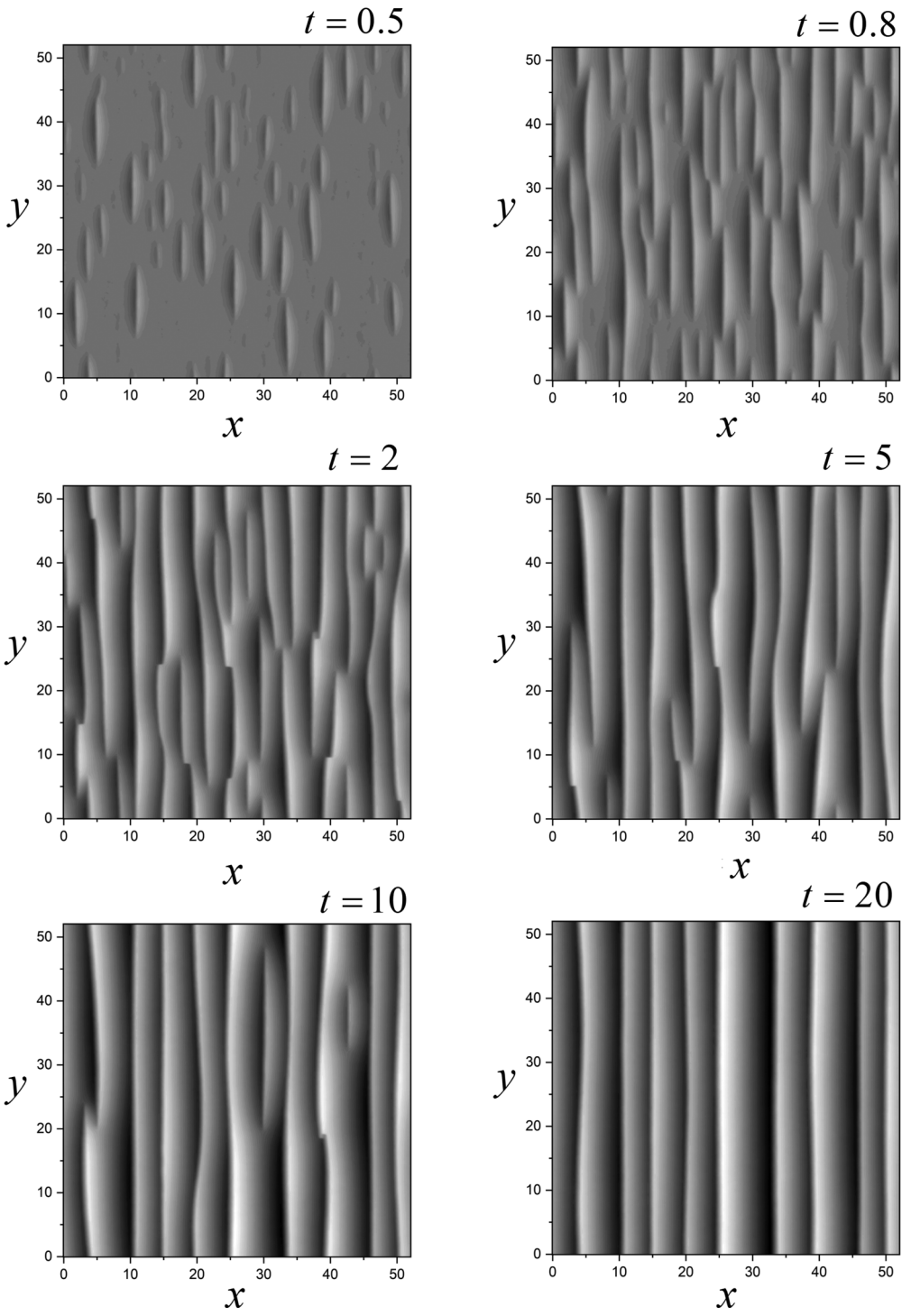

FIG. 10. Top view of the crystal surface, as defined by the isosurface $u = 0$, at various times.

anisotropic grain boundary motion [81], for instance. One could also use the model with a type-B dynamics (Cahn-Hilliard) to mimic surface diffusion in three dimensions, as proposed by Torabi *et al.* [30]. They showed using a matched asymptotic expansion method [30] that the model converges toward the equation for surface diffusion in two dimensions. This shall remain valid in three dimensions as well, whereas a formal analysis of the surface diffusion problem may be rather difficult.

ACKNOWLEDGMENT

This work was supported by the ANR FACET Project ANR-19-CE08-0014.

APPENDIX

For the derivation of the regularized stress tensor in the phase-field theory, consider the energy density

$\Lambda(\vec{x}, u, \vec{\nabla}u, \Delta u)$; which has explicit dependence on the scalar u, its gradient $\vec{\nabla}u$, its Laplacian Δu and the position vector $\vec{x}$. We have

$$d\Lambda = \frac{\partial \Lambda}{\partial x_j} dx_j + \frac{\partial \Lambda}{\partial u} du + \frac{\partial \Lambda}{\partial u_j} du_j + \frac{\partial \Lambda}{\partial \Delta u} d\Delta u, \tag{A1}$$

where we use the Einstein summation convention. x_j are the components of the position vector, and $u_j = \frac{\partial u}{\partial x_j}$. Differentiating with respect to x_k gives

$$\frac{d\Lambda}{dx_k} = \frac{\partial \Lambda}{\partial x_k} + \frac{\partial \Lambda}{\partial u} u_k + \frac{\partial \Lambda}{\partial u_j} u_{jk} + \frac{\partial \Lambda}{\partial \Delta u} \frac{\partial \Delta u}{\partial x_k}. \tag{A2}$$

We then use the Euler-Lagrange equation:

$$\frac{\partial \Lambda}{\partial u} - \vec{\nabla} \cdot \frac{\partial \Lambda}{\partial \vec{\nabla} u} + \Delta \left(\frac{\partial \Lambda}{\partial \Delta u} \right) = 0 \tag{A3}$$

in Eq. (A2) and obtain

$$\frac{d\Lambda}{dx_k} = \frac{\partial \Lambda}{\partial x_k} + \frac{d}{dx_j} \left(u_k \frac{\partial \Lambda}{\partial u_j} \right) + \frac{\partial \Lambda}{\partial \Delta u} \frac{\partial \Delta u}{\partial x_k} - u_k \frac{\partial^2}{\partial x_j \partial x_j} \left(\frac{\partial \Lambda}{\partial \Delta u} \right). \tag{A4}$$

We set $X = \frac{\partial \Lambda}{\partial \Delta u}$ and $Y = u_k$ and use the identity $X\Delta Y - Y\Delta X = -\vec{\nabla} \cdot (Y \vec{\nabla} X) + \vec{\nabla} \cdot (X \vec{\nabla} Y)$. Thus,

$$\frac{d\Lambda}{dx_k} - \frac{\partial \Lambda}{\partial x_k} = \vec{\nabla} \cdot \left(u_k \frac{\partial \Lambda}{\partial \vec{\nabla} u} \right) + \vec{\nabla} \cdot \left(\frac{\partial \Lambda}{\partial \Delta u} \vec{\nabla} u_k \right) - \vec{\nabla} \cdot \left(u_k \vec{\nabla} \frac{\partial \Lambda}{\partial \Delta u} \right). \tag{A5}$$

For energy density Λ that is not explicitly dependent of the position, as in the present model, we have $\frac{\partial \Lambda}{\partial x_k} = 0$. Equation (A5) holds for the three components of the vector position and therefore can be written as the divergence of a tensor:

$$0 = \vec{\nabla} \cdot \mathbf{S}, \tag{A6}$$

with

$$\mathbf{S} = \vec{\nabla} u \otimes \frac{\partial \Lambda}{\partial \vec{\nabla} u} - \Lambda \mathbf{I} + \frac{\partial \Lambda}{\partial \Delta u} \vec{\nabla} \vec{\nabla} u - \vec{\nabla} u \otimes \vec{\nabla} \frac{\partial \Lambda}{\partial \Delta u}. \tag{A7}$$

$\mathbf{I}$ is the unit tensor.

[1] W. W. Mullins, J. Appl. Phys. **27**, 900 (1956).
[2] W. Kingston, *The Physics of Powder Metallurgy* (Sylvaniaelectric Products, Inc., Danvers, MA, 1951).
[3] C. Herring, Phys. Rev. **82**, 87 (1951).
[4] M. E. Gurtin and M. E. Jabbour, Arch. Ration. Mech. Anal. **163**, 171 (2002).
[5] A. DiCarlo, M. E. Gurtin, and P. Podio-Guidugli, SIAM J. Appl. Math. **52**, 1111 (1992).
[6] G. Wulff, Z. Kristallogr. Crystal. Mater. **34**, 449 (1901).
[7] N. Cabrera, Surf. Sci. **2**, 320 (1964).
[8] W. K. Burton, N. Cabrera, and F. C. Frank, Philos. Trans. R. Soc. Lond. A **243**, 299 (1951).
[9] A. F. Andreev, Zh. Eksp. Teor. Phys. **80**, 2042 (1981).
[10] J. E. Taylor and J. W. Cahn, Physica D **112**, 381 (1998).
[11] A. Golovin, S. Davis, and A. Nepomnyashchy, Physica D **122**, 202 (1998).
[12] A. Golovin, S. Davis, and A. Nepomnyashchy, J. Cryst. Growth **198-199**, 1245 (1999).
[13] B. J. Spencer, Phys. Rev. E **69**, 011603 (2004).
[14] A. Mastroberardino and B. J. Spencer, IMA J. Appl. Math. **75**, 190 (2010).
[15] D. W. Hoffman and J. W. Cahn, Surf. Sci. **31**, 368 (1972).
[16] J. Cahn and D. Hoffman, Acta Metall. **22**, 1205 (1974).
[17] A. A. Golovin, S. H. Davis, and A. A. Nepomnyashchy, Phys. Rev. E **59**, 803 (1999).
[18] F. Liu and H. Metiu, Phys. Rev. B **48**, 5808 (1993).
[19] J. Stewart and N. Goldenfeld, Phys. Rev. A **46**, 6505 (1992).
[20] S. J. Watson, Proc. R. Soc. A **471**, 20140560 (2015).
[21] T. Philippe, H. Henry, and M. Plapp, J. Cryst. Growth **503**, 20 (2018).
[22] S. Watson, F. Otto, B. Rubinstein, and S. Davis, Physica D **178**, 127 (2003).
[23] T. V. Savina, A. A. Golovin, S. H. Davis, A. A. Nepomnyashchy, and P. W. Voorhees, Phys. Rev. E **67**, 021606 (2003).
[24] C. Ograin and J. Lowengrub, Phys. Rev. E **84**, 061606 (2011).
[25] S. J. Watson and S. A. Norris, Phys. Rev. Lett. **96**, 176103 (2006).
[26] S. J. Watson, Europhys. Lett. **118**, 56001 (2017).
[27] S. M. Wise, J. S. Lowengrub, J. S. Kim, K. Thornton, P. W. Voorhees, and W. C. Johnson, Appl. Phys. Lett. **87**, 133102 (2005).
[28] S. Wise, J. Kim, and J. Lowengrub, J. Comput. Phys. **226**, 414 (2007).
[29] A. Wheeler, Proc. R. Soc. A **462**, 3363 (2006).
[30] S. Torabi, J. Lowengrub, A. Voigt, and S. Wise, Proc. R. Soc. A **465**, 1337 (2009).
[31] A. K. Boukellal, A. K. Sidi Elvalli, and J.-M. Debierre, J. Cryst. Growth **522**, 37 (2019).
[32] P. Bollada, P. Jimack, and A. Mullis, Comput. Mater. Sci. **144**, 76 (2018).
[33] J.-M. Debierre, A. Karma, F. Celestini, and R. Guérin, Phys. Rev. E **68**, 041604 (2003).
[34] G. Demange, H. Zapolsky, R. Patte, and M. Brunel, Phys. Rev. E **96**, 022803 (2017).
[35] G. Demange, H. Zapolsky, R. Patte, and M. Brunel, npj Comput. Mater. **3**, 15 (2017).
[36] M. Salvalaglio, R. Backofen, R. Bergamaschini, F. Montalenti, and A. Voigt, Cryst. Growth Des. **15**, 2787 (2015).

[37] F. Abdeljawad, D. L. Medlin, J. A. Zimmerman, K. Hattar, and S. M. Foiles, J. Appl. Phys. **119**, 235306 (2016).
[38] N. Ofori-Opoku, J. A. Warren, and P. W. Voorhees, Phys. Rev. Mater. **2**, 083404 (2018).
[39] J. Eggleston and P. Voorhees, Appl. Phys. Lett. **80**, 306 (2002).
[40] J. Eggleston, G. McFadden, and P. Voorhees, Physica D **150**, 91 (2001).
[41] E. D. WILLIAMS and N. C. BARTELT, Science **251**, 393 (1991).
[42] P. Loreti and R. March, Eur. J. Appl. Math. **11**, 203 (2000).
[43] Q. Du, C. Liu, and X. Wang, J. Comput. Phys. **198**, 450 (2004).
[44] Q. Du, C. Liu, R. Ryham, and X. Wang, Nonlinearity **18**, 1249 (2005).
[45] X. Wang, SIAM J. Math. Anal. **39**, 1367 (2008).
[46] M. Röger and R. Schatzle, Math. Z. **254**, 675 (2006).
[47] E. De Giorgi, Some remarks on γ-convergence and least squares method, in *Composite Media and Homogenization Theory: An International Centre for Theoretical Physics Workshop*, edited by G. Dal Maso and G. F. Dell'Antonio (Birkhäuser Boston, Boston, MA, 1991), pp. 135–142.
[48] T. Philippe, H. Henry, and M. Plapp, Proc. R. Soc. A **476**, 20200227 (2020).
[49] A. A. Wheeler and G. B. McFadden, Proc. R. Soc. Lond. A **453**, 1611 (1997).
[50] G. B. McFadden, A. A. Wheeler, R. J. Braun, S. R. Coriell, and R. F. Sekerka, Phys. Rev. E **48**, 2016 (1993).
[51] A. A. Wheeler and G. B. McFadden, Eur. J. Appl. Math. **7**, 367 (1996).
[52] D. M. Anderson, G. B. McFadden, and A. A. Wheeler, Annu. Rev. Fluid Mech. **30**, 139 (1998).
[53] B. Nestler and A. A. Wheeler, Phys. Rev. E **57**, 2602 (1998).
[54] R. L. Pego and O. Penrose, Proc. R. Soc. Lond. A **422**, 261 (1989).
[55] G. Caginalp, in *Applications of Field Theory to Statistical Mechanics*, edited by L. Garrido (Springer, Berlin, 1985), pp. 216–226.
[56] T. Philippe, Phys. Rev. E **103**, 032801 (2021).
[57] D. M. Anderson and G. B. McFadden, in NIST IR 5887 *(National Institute of Standards and Technology*, Gaithersburg, MD, 1996).
[58] C. E. Weatherburn, *Differential Geometry of Three Dimensions*, Vol. 1 (Cambridge University Press, Cambridge, 1955).
[59] J. W. Cahn, C. M. Elliott, and A. Novick-Cohen, Eur. J. Appl. Math. **7**, 287 (1996).
[60] R. F. Sekerka, J. Cryst. Growth **275**, 77 (2005).
[61] J. R. Heffelfinger and C. Carter, Surf. Sci. **389**, 188 (1997).
[62] D. Knoppik and A. Lösch, J. Cryst. Growth **34**, 332 (1976).
[63] N. Reinecke and E. Taglauer, Surf. Sci. **454-456**, 94 (2000).
[64] Y. Kim, M. H. Jo, T. C. Kim, C. W. Yang, J. W. Kim, J. S. Hwang, D. Y. Noh, N. D. Kim, and J. W. Chung, Phys. Rev. Lett. **102**, 156103 (2009).
[65] S. Song, M. Yoon, S. Mochrie, G. Stephenson, and S. Milner, Surf. Sci. **372**, 37 (1997).
[66] W. Zhang, P. Sachenko, and I. Gladwell, Acta Mater. **52**, 107 (2004).
[67] W. Zhang and I. Gladwell, J. Cryst. Growth **277**, 608 (2005).
[68] F. Abdeljawad, S. M. Foiles, A. P. Moore, A. R. Hinkle, C. M. Barr, N. M. Heckman, K. Hattar, and B. L. Boyce, Acta Mater. **158**, 440 (2018).
[69] V. I. Marchenko, Zh. Eksp. Teor. Fiz **81**, 1141 (1981).
[70] H. Wang, A. S. Y. Chan, W. Chen, P. Kaghazchi, T. Jacob, and T. E. Madey, ACS Nano **1**, 449 (2007).
[71] H. Wang, W. Chen, and R. A. Bartynski, Surf. Sci. **635**, 85 (2015).
[72] W. Chen, H. Wang, and R. A. Bartynski, in *Catalysis by Materials with Well-Defined Structures*, edited by Z. Wu and S. H. Overbury (Elsevier, Amsterdam, 2015), pp. 301–338.
[73] M. Siegert, Phys. Rev. Lett. **81**, 5481 (1998).
[74] D. Moldovan and L. Golubovic, Phys. Rev. E **61**, 6190 (2000).
[75] G. Ehrlich and F. G. Hudda, J. Chem. Phys. **44**, 1039 (1966).
[76] R. L. Schwoebel, J. Appl. Phys. **40**, 614 (1969).
[77] W. W. Mullins, Philos. Mag. **6**, 1313 (1961).
[78] J. Krug, Adv. Phys. **46**, 139 (1997).
[79] H.-C. Jeong and J. D. Weeks, Phys. Rev. Lett. **75**, 4456 (1995).
[80] H. Hibino, Y. Homma, and T. Ogino, Phys. Rev. B **51**, 7753 (1995).
[81] M. Salvalaglio, D. J. Srolovitz, and J. Han, Acta Mater. **227**, 117463 (2022).